

Observation of Quantum Anomalous Hall Effect and Exchange Interaction in Topological Insulator/Antiferromagnet Heterostructure

Lei Pan, Alexander Grutter, Peng Zhang, Xiaoyu Che, Tomohiro Nozaki, Alex Stern, Mike Street, Bing Zhang, Brian Casas, Qing Lin He, Eun Sang Choi, Steven M. Disseler, Dustin A. Gilbert, Gen Yin, Qiming Shao, Peng Deng, Yingying Wu, Xiaoyang Liu, Xufeng Kou, Sahashi Masashi, Xiaodong Han, Christian Binek, Scott Chambers, Jing Xia, and Kang L. Wang*

Integration of a quantum anomalous Hall insulator with a magnetically ordered material provides an additional degree of freedom through which the resulting exotic quantum states can be controlled. Here, an experimental observation is reported of the quantum anomalous Hall effect in a magnetically-doped topological insulator grown on the antiferromagnetic insulator Cr_2O_3 . The exchange coupling between the two materials is investigated using field-cooling-dependent magnetometry and polarized neutron reflectometry. Both techniques reveal strong interfacial interaction between the antiferromagnetic order of the Cr_2O_3 and the magnetic topological insulator, manifested as an exchange bias when the sample is field-cooled under an out-of-plane magnetic field, and an exchange spring-like magnetic depth profile when the system is magnetized within the film plane. These results identify antiferromagnetic insulators as suitable candidates for the manipulation of magnetic and topological order in topological insulator films.

The recent realization of the quantum anomalous Hall effect (QAHE) in magnetically-doped 3D topological insulators (TIs) opens new possibilities for realizing dissipationless edge states without the application of an external magnetic field.^[1,2] With the introduction of magnetic dopants, the time-reversal symmetry of the topological surface states is broken, and the resulting magnetic exchange gap has led to a series of exotic physical phenomena.^[3–5] At the same time, the engineering of TI-based magnetic heterostructures has greatly broadened opportunities for deterministic manipulation of the topological and magnetic order as the interfacial discontinuities yield a complex and highly tunable energy landscape.^[6,7] For example,

Dr. L. Pan, P. Zhang, Dr. X. Che, Prof. Q. L. He, Dr. G. Yin, Prof. Q. Shao, Dr. P. Deng, Y. Wu, Prof. K. L. Wang
Department of Electrical and Computer Engineering
University of California
Los Angeles, CA 90095, USA
E-mail: wang@ee.ucla.edu

Dr. A. Grutter, Dr. S. M. Disseler
NIST Center for Neutron Research
National Institute of Standards and Technology
Gaithersburg, MD 20899-6102, USA

Dr. T. Nozaki, Prof. S. Masashi
Department of Electronic Engineering
Tohoku University
Sendai 980-8579, Japan

Dr. A. Stern, Dr. B. Casas, Prof. J. Xia
Department of Physics and Astronomy
University of California
Irvine, CA 92697, USA

Dr. M. Street, Prof. C. Binek
Department of Physics and Astronomy
University of Nebraska
Lincoln, NE 68588, USA

Dr. B. Zhang, Prof. X. Han
Beijing Key Lab of Microstructure and Property of Advanced Materials
Beijing University of Technology
Beijing 100124, China


Prof. Q. L. He
International Center for Quantum Materials
School of Physics
Peking University
Beijing 100871, China

Prof. E. S. Choi
National High Magnetic Field Laboratory
Florida State University
Tallahassee, FL 32310-3706, USA

Prof. D. A. Gilbert
Department of Materials Science
University of Tennessee
Knoxville, TN 37996, USA

Prof. Q. Shao
Department of Electronic and Computer Engineering
The Hong Kong University of Science and Technology
Clear Water Bay, Kowloon, Hong Kong SAR, China

X. Liu, Prof. X. Kou
School of Information Science and Technology
ShanghaiTech University
Shanghai 200031, China

 The ORCID identification number(s) for the author(s) of this article can be found under <https://doi.org/10.1002/adma.202001460>.

DOI: 10.1002/adma.202001460

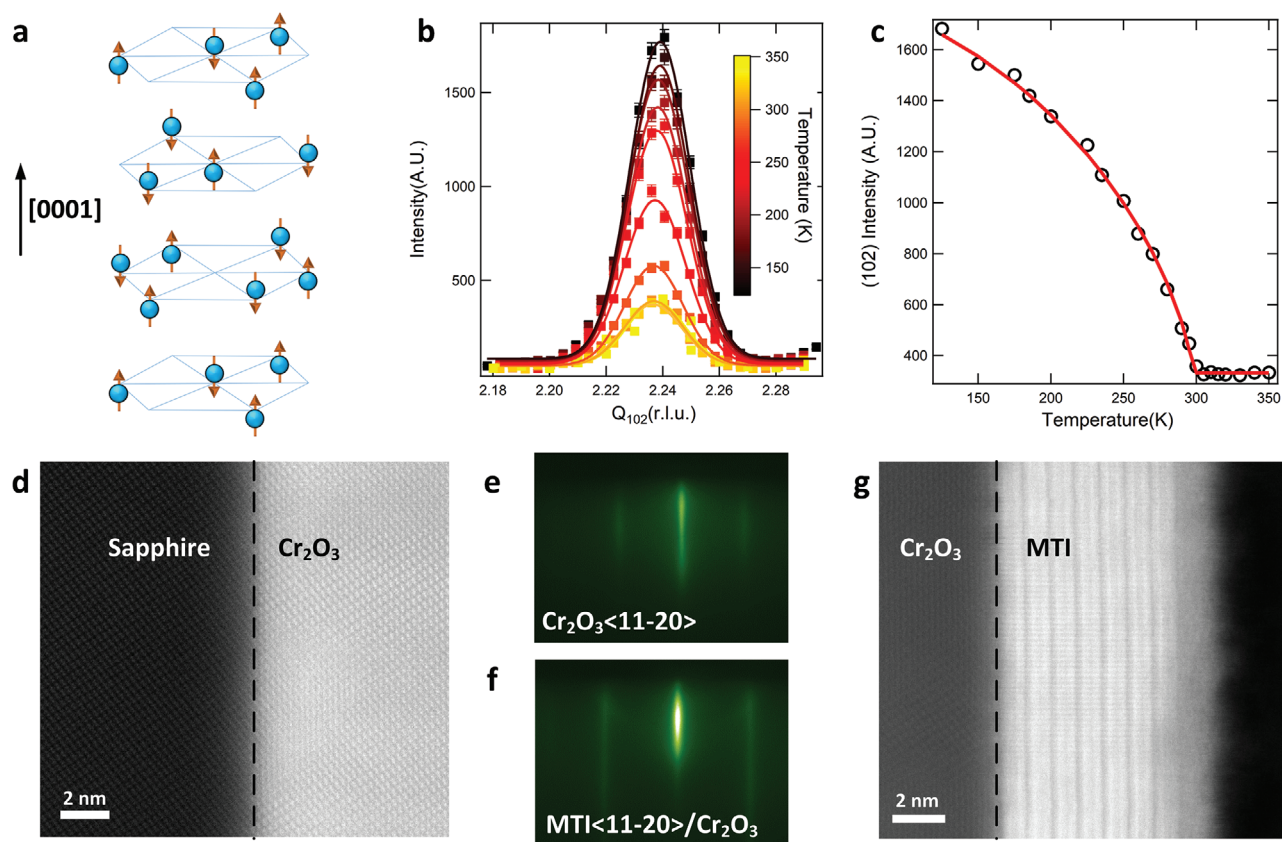


Figure 1. High quality quantum anomalous Hall insulator grown by molecular beam epitaxy on $\text{Cr}_2\text{O}_3(0001)$. a) Spin structure of antiferromagnet Cr_2O_3 (only Cr atoms are shown). Cr atoms show a buckled arrangement. b) Neutron diffraction measurement of the Cr_2O_3 ($H\ 0\ 2H$) for temperature ranging from 125 to 350 K. c) Fitting the data reveals a T_N value of 297 K. d) HAADF-STEM of the Cr_2O_3 /sapphire interface. e, f) RHEED pattern of the MBE grown Cr_2O_3 and MTI on Cr_2O_3 . g) HAADF-STEM of the MTI/ Cr_2O_3 heterostructure.

the integration of a QAH insulator with a superconductor leads to chiral Majorana edge modes.^[8,9] Additionally, the growth of multilayer QAH insulators spaced by the normal insulator CdSe results in an artificial high-Chern-number QAH insulator.^[10] While most functional heterostructures have mainly focused on control of the topological nature of the QAH insulator, the use of magnetic couplings in such hybrid systems to manipulate the QAH state remains unexplored. There are two major challenges in the quest to realize a magnetically-ordered heterostructure based on a QAH insulator. First, the material must be highly insulating to avoid current shunting effects. Second, the critical growth requirements for achieving the QAHE mandate the selected magnetic material be compatible

with the QAH insulator. In addition, it is highly desirable that the adjacent magnetic layer enable the effective manipulation of the magnetic or topological order in the QAH insulator, either through direct interfacial exchange (e.g., exchange bias) coupling or via the magnetoelectric effect.

An ideal candidate to address these longstanding challenges is Cr_2O_3 , an antiferromagnetic (AFM) insulator with a Néel temperature (T_N) near 300 K.^[11] As shown in **Figure 1a**, the Cr spins in Cr_2O_3 are generally thought to align parallel or antiparallel to $[0001]$, resulting in robust antiferromagnetic ordering along the c -axis, and alternating rows of ferromagnetically aligned spins in the basal plane. Experimentally, high-quality Cr_2O_3 can be readily grown on the $\text{Al}_2\text{O}_3(0001)$ via either sputtering, pulsed laser deposition, or molecular beam epitaxy (MBE), as the two materials have similar lattice constants and the same crystal symmetry.^[12–14] Given our previous experience of the $\text{Cr}:(\text{Bi},\text{Sb})_2\text{Te}_3$ growth on the $\text{Al}_2\text{O}_3(0001)$ substrate,^[15] the realization of a QAH insulator on Cr_2O_3 is thus feasible. Furthermore, Cr_2O_3 is a magnetoelectric material in which a net magnetic moment can be induced by applying an electric field. If properly utilized, this property can be used to electrically manipulate the magnetic states of an adjacent exchange-coupled ferromagnetic material, enabling electric-field-controlled exchange bias.^[16,17]

In this study, we demonstrate the epitaxial growth of the magnetic topological insulator (MTI) $\text{Cr}:(\text{Bi},\text{Sb})_2\text{Te}_3$ on an

Dr. S. Chambers
Physical and Computational Sciences Directorate
Pacific Northwest National Laboratory
Richland, WA 99352, USA

Prof. K. L. Wang
Department of Materials Science and Engineering
University of California
Los Angeles, CA 90095, USA

Prof. K. L. Wang
Department of Physics
University of California
Los Angeles, CA 90095, USA

epitaxial film of Cr₂O₃(0001) with high crystallinity. Well-defined magnetic and antiferromagnetic orders are confirmed by neutron diffraction. Significantly, the MTI/Cr₂O₃ heterostructure exhibits the QAHE at low-temperature where dissipationless chiral edge conduction is achieved. In addition, by using field cooling and depth-sensitive polarized neutron reflectometry techniques, we reveal the presence of exchange bias in the system as a result of strong interfacial exchange coupling. Our work thus provides a new platform to study the interactions of a QAH insulator with an antiferromagnet and reveals new opportunities for functionalizing and manipulating macroscopic quantum states via coupling to antiferromagnetic order.

Most QAH insulators have been grown on traditional semiconductor substrates (e.g., InP and GaAs^[18–20]) to achieve the highest film quality, or on complex oxides (e.g., SrTiO₃^[21]) to gain control of the thin film's chemical potential through back-gating. By carefully tuning the growth parameters, we successfully achieved a high-quality interface of an MTI with (0001)-oriented Cr₂O₃ on a Al₂O₃ substrate.

Cr₂O₃ films were deposited by either MBE or sputtering on α -Al₂O₃(0001) with thicknesses of 40 nm and 1 μ m. We did not observe obvious material quality difference when growing MTI on these two kinds of substrate as explained in the Supporting Information. To verify the antiferromagnetic state of these films, we performed temperature-dependent neutron diffraction on the (102) magnetic reflection, as shown in Figure 1b. Measurements were performed sputter-grown thin films using the SPINS instrument at the NIST Center for Neutron Research over the temperature range 125 to 350 K. Fitting the data (Figure 1c) reveals a Néel temperature of 297.3 \pm 0.3 K, in excellent agreement with the bulk value, thus confirming the

realization of high-quality bulk-like antiferromagnetic Cr₂O₃ films. Additionally, an atomically sharp interface between the Al₂O₃ and Cr₂O₃ layer is clearly seen by using high-angle annular dark field (HAADF) scanning transmission electron microscopy (STEM), as seen in Figure 1d.

The subsequent MTI growth was performed in a different MBE chamber after cleaning the Cr₂O₃ surface. The epitaxial growth of 7 quintuple-layers (QL) of high-quality Cr:(Bi,Sb)₂Te₃ thin films was confirmed by the observation of a reflective high-energy electron diffraction (RHEED) pattern with sharp, unmodulated streaks, indicating 2D growth as shown in Figure 1e,f. A clear boundary across the chromia/MTI interface and the well-defined van der Waals structure of the MTI are seen in Figure 1g.

Remarkably, by optimizing the growth conditions,^[19] we are able to observe the QAHE in MTI/Cr₂O₃ heterostructures (this sample will be referred to as sample 1). As illustrated in Figure 2a,b, the Hall resistivity reaches the quantized state at $\rho_{yx} = 1 \frac{h}{e^2}$ (h is Planck's constant and e as the electron charge) when the sample is cooled down to 20 mK, and the longitudinal resistivity drops to below $0.1 \frac{h}{e^2}$. Using the conductance tensor to convert resistivity to conductivity, we obtain evidence for the quantum phase transition (Figure 2c). The semicircular characteristic in the (σ_{xy}, σ_{xx}) conductance plot continuously connects the two quantized points at $(\sigma_{xy}, \sigma_{xx}) = (\pm \frac{e^2}{h}, 0)$, thereby demonstrating the quantum transport feature characteristic of the QAHE.^[22]

To shed light on the magnetic interaction between the AFM Cr₂O₃ film and the top MTI layer in the QAHE state, we probed

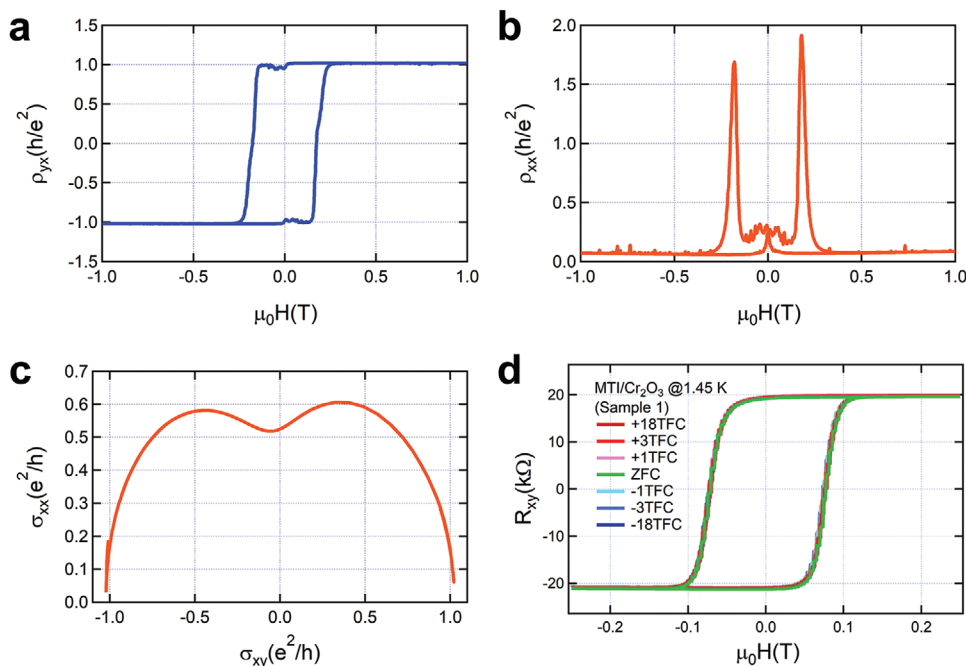


Figure 2. Observation of quantum anomalous Hall effect in MTI/Cr₂O₃ heterostructure. Hall a) and longitudinal resistivity b) for an MTI/Cr₂O₃ Hall-bar measured at 20 mK. The Hall resistance reached a value of $1 \frac{h}{e^2}$. c) Evolution of the longitudinal conductivity σ_{xx} versus σ_{xy} when the magnetic field is swept between two saturation states (+2T and -2T). The semicircular behavior between the points $(\pm \frac{e^2}{h}, 0)$ reveals the quantum Hall state transition. d) Hysteresis loop at 1.45 K of sample 1 after different field cooling conditions, no exchange bias shift was observed in this sample.

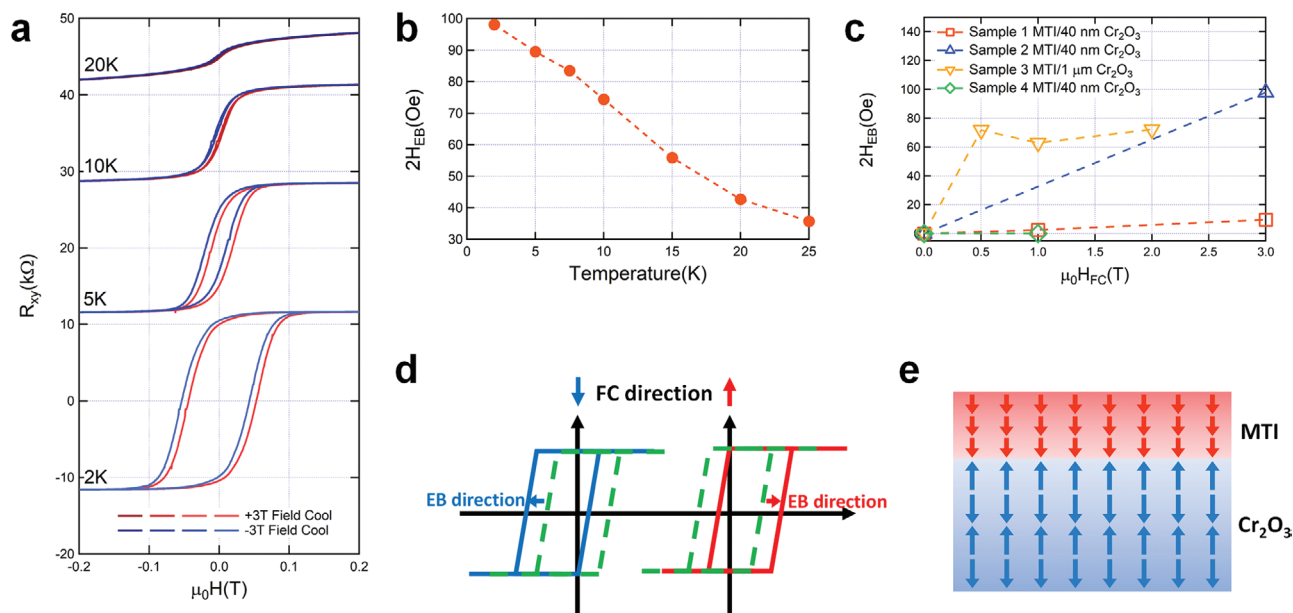


Figure 3. Exchange bias effect in MTI/Cr₂O₃ heterostructure. a) Temperature dependent hysteresis loops and b) summarized temperature dependent exchange bias field size of sample 2 after different magnetic field coolings. c) Exchange bias field summary of sample 1 to 4 using different field cooling field. d) Schematic diagram illustrating positive exchange bias. e) Schematic spin alignment at the MTI/Cr₂O₃ interface; the positive exchange bias sign is because of the antiparallel alignment of spins at the interface.

the interface using both exchange bias and polarized neutron reflectometry (PNR) measurements. For the former, we performed a series of magneto-transport measurements under different field cooling conditions. The sample was first heated to 320 K (i.e., above the T_N of Cr₂O₃ of 297 K), at which point a perpendicular magnetic field ranging from +3 to -3 T was applied, followed by cooling to 1.45 K. Once the base temperature was reached, anomalous Hall measurements were performed to capture the hysteresis loop shift due to exchange bias. Surprisingly, the hysteresis loop for sample 1 under different field cooling conditions exhibits no obvious exchange bias, as seen in Figure 2d. For comparison, we grew several MTIs (sample 2/3/4) on Cr₂O₃ with the same thickness. Their transport results are shown in Figure 3a, Figure S10a,b in the Supporting Information, respectively. In sample 2, a pronounced exchange bias field was observed by using two opposite magnetic field coolings (+3 and -3 T) as evidenced by the horizontal hysteresis loop shift as shown in Figure 3a. The exchange bias field remains visible until the temperature rises above the Curie temperature (≈ 30 K) of the MTI thin film. In sample 3 and 4 where 3 was grown on 1- μ m-thick Cr₂O₃ and 4 was grown on 40-nm-thick Cr₂O₃, again we saw different exchange bias behaviors: Sample 3 showed exchange bias and sample 4 did not as shown in Figure S10a,b in the Supporting Information. To rule out the potential carrier density dependency, we carried out the exchange bias experiment on sample 2 with the addition of a boron nitride top gate as shown in Figure S11b in the Supporting Information. However, we did not observe clear gate voltage dependence as shown in Figure S11a,c in the Supporting Information.

Here, we point out that although similar field-cooling measurements were performed, we observed large variations in terms of the exchange bias effect among these MTI/Cr₂O₃

samples as summarized in Figure 3c. Specifically, while two samples do exhibit exchange-biased hysteresis loops as shown in Figure 3a and Figure S10a (Supporting Information), the magnetic hysteresis loops remain almost symmetric under different field-cooling conditions in two other samples. Notably, we see that the measured exchange bias fields for both samples presented in Figure 3a and Figure S10a (Supporting Information) show the same sign as the applied magnetic field, as schematically illustrated in Figure 3d. This is known as positive exchange bias and it occurs when the hysteresis loop shifts to the positive (negative) field direction as a result of a positive (negative) applied field. Positive exchange bias is usually a result of antiparallel alignment between the AFM and MTI's surface spins, as shown schematically in Figure 3e.^[23]

Understanding the magnitude of the exchange bias remains an ongoing challenge for both theorists and experimentalists. For our MTI/Cr₂O₃ heterostructure, one of the possible factors responsible for the large exchange bias variations is the gap between MTI's low Curie temperature (≈ 30 K) and Cr₂O₃'s relatively higher Néel temperature. When temperature is cooled across the Néel temperature of Cr₂O₃, MTI remains in a random magnetization state which may create disorders in the Cr₂O₃'s magnetic boundary state. Similar result of the vanishing exchange bias in a Cr-doped Sb₂Te₃/Cr₂O₃ structure has also been reported recently.^[24] To overcome this issue, a magnetoelectric field cool process (applying out-of-plane magnetic field and electric field simultaneously during field cool) may be needed to achieve a robust single-domain boundary magnetization state in Cr₂O₃.^[12,16] Another possible factor is the varying densities of pinned or uncompensated spins at the interface. Previous studies have shown that the Cr₂O₃ surface has a unique surface boundary magnetization state that is related to the exchange bias magnitude.^[16,25,26] Under

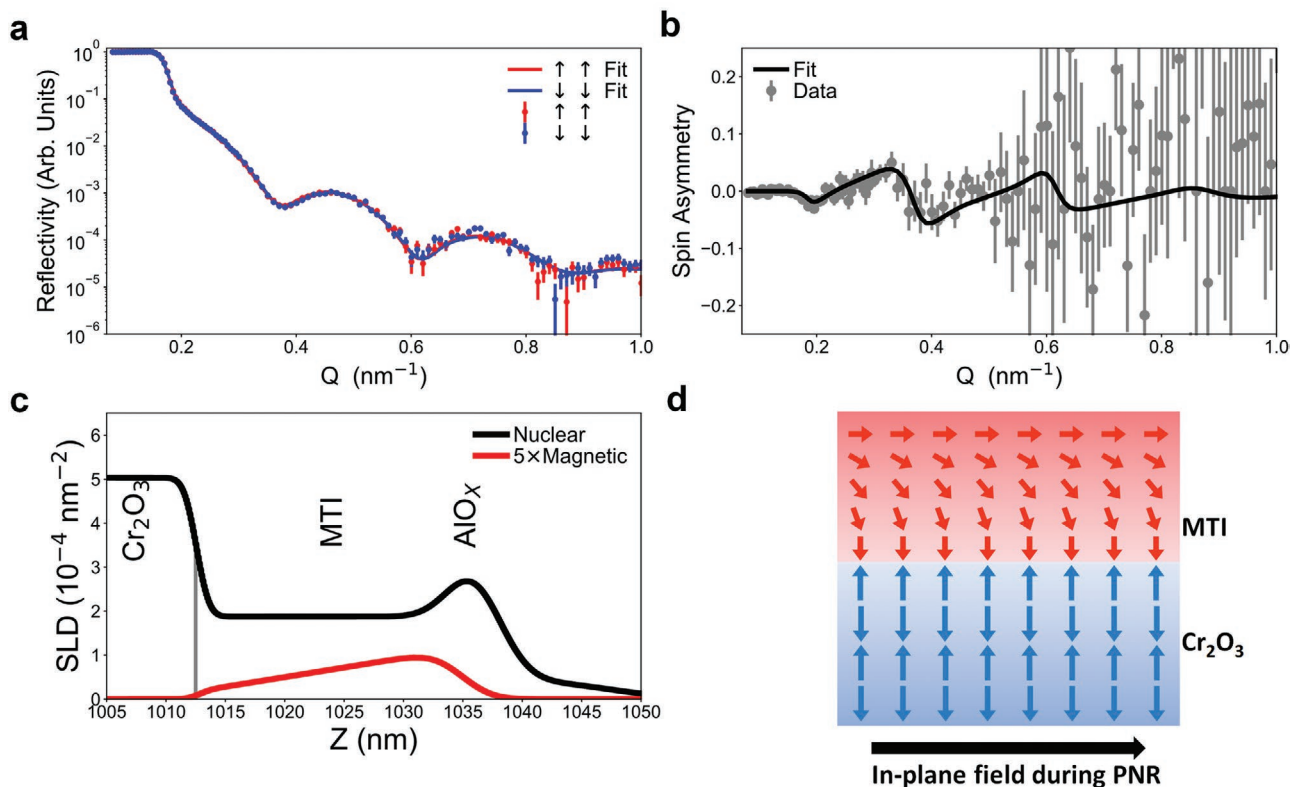


Figure 4. Capturing the exchange interaction between MTI and Cr_2O_3 by neutron techniques. a) Spin-dependent polarized-neutron reflectometry and b) spin asymmetry from an MTI/ $1\ \mu\text{m}$ Cr_2O_3 /Sapphire heterojunction in an applied in-plane field of 700 mT along with the best fit generated by the nuclear and c) magnetic depth profile models. d) Schematic drawing of magnetic depth profile shown in (c) where an in-plane field was applied.

such circumstances, when coupled to the MTI, the number of uncompensated spins pinned at the interface is expected to vary among different batches of MTI/ Cr_2O_3 samples and lead to variations in the exchange bias.

To more directly probe the magnetic coupling at the interface, we used PNR to determine the depth-resolved magnetization profile which in turn allows us to understand the strength and range of the spin coupling across the MTI/ Cr_2O_3 interface. Because PNR probes magnetization components pulled in-plane by the applied field, it is much less sensitive to the domain state at the interface, making it the ideal technique for extracting the coupling information at this complex interface. PNR measurements were performed using the PBR instrument at the NIST Center for Neutron Research as described in the methods section, and samples were again field cooled from above the Cr_2O_3 T_N . The neutron measurements were performed at 6 K with in-plane magnetic fields of 700 mT (results shown in Figure 4) and 3 T (results shown in Figures. S4–S7 in the Supporting Information). The sample used was grown in the same batch as sample 3 using the exact same growth condition and substrate except for the thicker MTI layer to facilitate the neutron measurement.

Figure 4a,b shows the spin-dependent neutron reflectivities and spin asymmetry (defined as the difference between the spin-polarized reflectivities divided by their sum), respectively, overlapped with the fit from a theoretical model for a measurement performed at the lower field of 700 mT. The converged model, shown in Figure 4c, is used to generate the calculated

reflectometry profiles which are an extremely good match to the data. The magnetization profile for the converged model is shown schematically in Figure 4d. The converged models confirm the very high-quality interfaces between the Cr_2O_3 and MTI, in agreement with the STEM shown in Figure 1g. Interestingly, models which match the splitting in the reflectivity, such as the one shown in Figure 4c, exhibit a nonuniform magnetization with a suppression of the magnetic scattering length-density (magnetic scattering length density (SLD), which is directly proportional to the in-plane projection of the magnetization) near the MTI/ Cr_2O_3 interface. We interpret this as shown by the schematic in Figure 4d, where the magnetization at the Cr_2O_3 /MTI interface, being oriented in the out-of-plane direction, is invisible to PNR and consequently does not contribute to the magnetic SLD. Since modeling of reflectivity data often produces multiple degenerate models which describe the data equally well, we evaluated a variety of candidate profiles, which are shown in the Supporting Information. Specifically, we considered models with uniform and linearly varying magnetization profiles, as well as models exhibiting an exponential decay of the magnetization towards a bulk-like value, or models with an interfacial dead layer. In all cases, we found that only a non-uniform magnetic SLD profile with suppressed magnetization at the MTI/ Cr_2O_3 interface can accurately capture the spin asymmetry shown in Figure 4b.

A reduction in the magnetic SLD approaching the Cr_2O_3 interface is found in both the low-field (700 mT) and high-field (3 T) PNR measurements, so that a nonuniform magnetization

is required to properly describe the splitting between the reflectivities for the two spin states. Only the linear or exponential models, which yield qualitatively similar profiles due to the smearing associated with long-range interface roughness, can accurately describe the data at both field values, with a slight preference for the linear model. It is critical to note that the profile measured in 3 T is more uniform than that of 700 mT and shows a larger magnetization near the Cr₂O₃ interface than is found at 700 mT, demonstrating that this is not simply a reduction in magnetic moment, but primarily a canting of the moments resulting from competition between the in-plane magnetic field and a perpendicular magnetic anisotropy. Although the PNR does not conclusively eliminate the possibility that a fraction of the magnetic SLD gradient originates in a truly nonuniform magnetization profile rather than entirely through spin-canting, we may address this question through energy dispersive X-ray spectroscopy, Figure S8 (Supporting Information), which does confirm that this is not an effect of a chromium gradient within the MTI. The winding of the magnetic moment observed by comparing the 700 mT and 3 T measurements is consistent with this picture and represents an exchange spring-like behavior.

The large perpendicular anisotropy in the MTI, demonstrated by the resistance of the magnetization to the applied 3 T field, is surprising given that the typical MTI has an anisotropy of <1 T. This observation suggests a very strong magnetic coupling between the AFM and the MTI. A natural explanation is that the uncompensated pinned moments on the surface of the Cr₂O₃, which have a strong *c*-axis anisotropy, couple to the moments in the MTI, forcing them out-of-plane. Although this explanation is consistent with the traditional understanding of exchange bias in which the orientation of the pinned moments is controlled by the AFM and is expected to be robust up to the exchange field, the orientation of the MTI would not typically be expected to reflect a similar strength. One possibility is that the Cr₂O₃ interface is comprised of a much larger pinned, uncompensated surface, consistent with the reconstructions previously discussed.^[16,25,26] These reconstructed surfaces could likely give many inclusions which did not undergo reconstruction and are strongly pinned to the AFM. These inclusions, along with the relatively weak sensitivity to the magnetic field due to the thin nature of the surface reconstruction, allow the surface to possess large areas of pinned uncompensated moments. As a result, the coupling between the Cr₂O₃ and the MTI is much stronger than the typical exchange bias effect. We note that the demonstrated magnetoelectricity of this reconstructed surface state suggests excellent potential for electric field control of the MTI in this system.

Thus, the PNR data corroborates very strong exchange coupling between the antiferromagnet and the MTI layers, potentially leading to ways to manipulate quantum anomalous Hall states and other topological properties.

In conclusion, we have successfully demonstrated the QAHE in an MTI/Cr₂O₃ heterostructure. We further confirm exchange coupling exists in the same material system between MTI and Cr₂O₃ using field-cooling magnetometry and PNR measurements. The exchange bias effects observed in different field-cooling schemes reveal a strong antiparallel coupling of magnetic moments across the interface. The PNR results

further support the coupling scenario with a detailed magnetization profile. As an outlook, the potential interplay between quantum anomalous Hall states and exchange bias effect in this system may provide an additional degree of freedom through which we may manipulate the quantum states for use in spintronics and low-dissipation electronics.

Experimental Section

Epitaxial Growth: Single-crystal Cr₂O₃ thin films are received using three different growth techniques. Much variation in terms of material quality and exchange interaction behavior was not observed in MTI/Cr₂O₃ heterostructures. The quantum anomalous Hall sample was grown on MBE-grown Cr₂O₃ films. The (0001)-oriented α -Cr₂O₃ epitaxial films were grown by MBE at PNNL using a high-temperature effusion cell with 5N purity Cr metal and an electron cyclotron resonance oxygen plasma source. The substrate temperature was 650 °C. Other experiment is based on Cr₂O₃ grown by reactive sputtering in an Ar and O₂ mixture gas at 500 °C. Thin films grown by pulsed laser deposition was also received from a chromia target and the substrate temperature was kept at 700 °C. However, this manuscript does not include transport or neutron results based on these samples.

The Cr₂O₃ samples were then transferred through air to UCLA where MTI thin films were grown by MBE in an ultrahigh vacuum Perkin–Elmer system. Following sonication in acetone and DI water, the samples were loaded into the Perkin–Elmer system and heated to 500 °C for 1 h to clean the surfaces. During MTI growth, the α -Cr₂O₃/ α -Al₂O₃ (0001) specimens were maintained at 220 °C growth temperature with 6N purity Bi, Sb, Te, and Cr elements coevaporated from Knudsen cells. The epitaxial growths were monitored in situ by RHEED to optimize the growth conditions. The MTI composition is (Cr_{0.12}Bi_{0.26}Sb_{0.62})₂Te₃ which is similar to the previous QAHE related work because of similar growth conditions.^[22]

Transport Measurements: Magneto-transport was performed in both He3/He4 dilution fridge, SCM2 system at the National High Magnetic Field Lab and PPMS. 10 nA AC current was applied by sourcing 1 V RMS across a 100 M Ω reference resistor at 7.351 Hz measurement frequency. The drain current, longitudinal voltage (V_{xx}) and Hall voltage (V_{yx}) were measured with SR830 lock-in amplifiers.

Polarized Neutron Reflectometry: Samples were field cooled in an in-plane applied field of either 700 mT or 3 T to the temperature of 6 K. Measurements were performed in the specular reflection geometry, with the direction of wave vector transfer perpendicular to the superlattice surface. The neutron propagation direction was perpendicular to the applied field direction. Based on the strong perpendicular anisotropy of MTI films, any magnetization not pointing along the applied field is expected to lie in the out-of-plane direction, so that, spin-flip scattering is not expected. Therefore, the spin-up and spin-down reflectivities were obtained using full polarization analysis to ensure that the incident and scattered beams retained identical neutron polarization directions. It is referred, therefore, only to the spin-up and spin-down nonspin-flip reflectivities, which are a function of the nuclear and magnetic SLD profiles. Fitting of the data allows the structural and magnetic depth profiles to be deduced, and modeling was performed using the NIST Refl1d software package.^[27] Data reduction was performed with the Reductus software package.^[28]

Supporting Information

Supporting Information is available from the Wiley Online Library or from the author.

Acknowledgements

L.P., A.G., and P.Z. contributed equally to this work. This work is supported as part of the Spins and Heat in Nanoscale Electronic

Systems (SHINES), an Energy Frontier Research Center funded by the US Department of Energy (DOE), Office of Science, Basic Energy Sciences (BES), under Award No. DE-SC0012670. The authors acknowledge the support from the Army Research Office Multidisciplinary University Research Initiative (MURI) program accomplished under Grant Number W911NF-16-1-0472 and W911NF-15-1-10561. The work at PNNL was supported by the U.S. Department of Energy, Office of Science, Division of Materials Sciences and Engineering under Award No. 10122. The PNNL work was performed in the Environmental Molecular Sciences Laboratory, a national scientific user facility sponsored by the Department of Energy's Office of Biological and Environmental Research and located at PNNL. This work used the Extreme Science and Engineering Discovery Environment (XSEDE), which is supported by National Science Foundation Grant Number ACI-1053575. Specifically, it used the Darter Cray XC30 system and the Bridges system, which is supported by NSF Award Number ACI-1445606, at the Pittsburgh Supercomputing Center (PSC). This research used resources of the Advanced Light Source, which is a DOE Office of Science User Facility under Contract No. DE-AC02-05CH11231. X.F.K acknowledges the support from the 1000-Young talent program of China, the National Key R&D Program of China under contract number 2017YFB0405704, and the Shanghai Sailing program under contract number 17YF1429200. The work at UC Irvine was supported by NSF grant DMR-1807817. A portion of this work was performed at the National High Magnetic Field Laboratory, which is supported by the National Science Foundation Cooperative Agreement No. DMR-1157490, No. DMR-1644779 and the State of Florida. Q.L.H. acknowledges the supports from the National Natural Science Foundation of China (Grant No. 11874070), the National Key R&D Program of China (Grant No. 2018YFA0305601), the Strategic Priority Research Program of Chinese Academy of Sciences (Grant No. XDB28000000), and National Thousand-Young Talents Program in China.

Conflict of Interest

The authors declare no conflict of interest.

Keywords

antiferromagnet, quantum anomalous Hall effect, topological insulators

Received: February 29, 2020

Revised: June 15, 2020

Published online: July 21, 2020

- [1] R. Yu, W. Zhang, H.-J. Zhang, S.-C. Zhang, X. Dai, Z. Fang, *Science* **2010**, 329, 61.
- [2] C.-Z. Chang, J. Zhang, X. Feng, J. Shen, Z. Zhang, M. Guo, K. Li, Y. Ou, P. Wei, L.-L. Wang, Z.-Q. Ji, Y. Feng, S. Ji, X. Chen, J. Jia, X. Dai, Z. Fang, S.-C. Zhang, K. He, Y. Wang, L. Lu, X.-C. Ma, Q.-K. Xue, *Science* **2013**, 340, 167.
- [3] H. Z. Lu, W. Y. Shan, W. Yao, Q. Niu, S. Q. Shen, *Phys. Rev. B* **2010**, 81, 115407.
- [4] R. Li, J. Wang, X.-L. Qi, S.-C. Zhang, *Nat. Phys.* **2010**, 6, 284.
- [5] Y. Fan, P. Upadhyaya, X. Kou, M. Lang, S. Takei, Z. Wang, J. Tang, L. He, L.-T. Chang, M. Montazeri, G. Yu, W. Jiang, T. Nie, R. N. Schwartz, Y. Tserkovnyak, K. L. Wang, *Nat. Mater.* **2014**, 13, 699.
- [6] Q. L. He, G. Yin, L. Yu, A. J. Grutter, L. Pan, C.-Z. Chen, X. Che, G. Yu, B. Zhang, Q. Shao, A. L. Stern, B. Casas, J. Xia, X. Han, B. J. Kirby, R. K. Lake, K. T. Law, K. L. Wang, *Phys. Rev. Lett.* **2018**, 121, 096802.
- [7] Q. L. He, G. Yin, A. J. Grutter, L. Pan, X. Che, G. Yu, D. A. Gilbert, S. M. Disseler, Y. Liu, P. Shafer, B. Zhang, Y. Wu, B. J. Kirby, E. Arenholz, R. K. Lake, X. Han, K. L. Wang, *Nat. Commun.* **2018**, 9, 2767.
- [8] J. Wang, Q. Zhou, B. Lian, S. C. Zhang, *Phys. Rev. B* **2015**, 92.
- [9] Q. L. He, L. Pan, A. L. Stern, E. C. Burks, X. Che, G. Yin, J. Wang, B. Lian, Q. Zhou, E. S. Choi, K. Murata, X. Kou, Z. Chen, T. Nie, Q. Shao, Y. Fan, S.-C. Zhang, K. Liu, J. Xia, K. L. Wang, *Science* **2017**, 357, 294.
- [10] G. Y. Jiang, Y. Feng, W. X. Wu, S. R. Li, Y. H. Bai, Y. X. Li, Q. H. Zhang, L. Gu, X. Feng, D. Zhang, C. Song, L. Wang, W. Li, X.-C. Ma, Q.-K. Xue, Y. Wang, K. He, *Chin. Phys. Lett.* **2018**, 35, 076802.
- [11] N. Wu, X. He, A. L. Wysocki, U. Lanke, T. Komatsu, K. D. Belashchenko, C. Binek, P. A. Dowben, *Phys. Rev. Lett.* **2011**, 106.
- [12] T. Ashida, M. Oida, N. Shimomura, T. Nozaki, T. Shibata, M. Sahashi, *Appl. Phys. Lett.* **2014**, 104, 152409.
- [13] M. Street, W. Echtenkamp, Takashi Komatsu, Shi Cao, P. A. Dowben, Ch. Binek, *Appl. Phys. Lett.* **2014**, 104, 222402.
- [14] M. A. Henderson, S. A. Chambers, *Surf. Sci.* **2000**, 449, 135.
- [15] X. Che, K. Murata, L. Pan, Q. L. He, G. Yu, Q. Shao, G. Yin, P. Deng, Y. Fan, B. Ma, X. Liang, B. Zhang, X. Han, L. Bi, Q.-H. Yang, H. Zhang, K. L. Wang, *ACS Nano* **2018**, 12, 5042.
- [16] X. He, Y. Wang, N. Wu, A. N. Caruso, E. Vescovo, K. D. Belashchenko, P. A. Dowben, C. Binek, *Nat. Mater.* **2010**, 9, 579.
- [17] T. Ashida, M. Oida, N. Shimomura, T. Nozaki, T. Shibata, M. Sahashi, *Appl. Phys. Lett.* **2015**, 106, 132407.
- [18] M. Mogi, M. Kawamura, R. Yoshimi, A. Tsukazaki, Y. Kozuka, N. Shirakawa, K. S. Takahashi, M. Kawasaki, Y. Tokura, *Nat. Mater.* **2017**, 16, 516.
- [19] X. F. Kou, S. T. Guo, Y. B. Fan, L. Pan, M. R. Lang, Y. Jiang, Q. Shao, T. Nie, K. Murata, J. Tang, Y. Wang, L. He, T. K. Lee, W. L. Lee, K. L. Wang, *Phys. Rev. Lett.* **2014**, 113, 137201.
- [20] M. Mogi, M. Kawamura, R. Yoshimi, A. Tsukazaki, Y. Kozuka, N. Shirakawa, K. S. Takahashi, M. Kawasaki, Y. Tokura, *Nat. Mater.* **2017**, 16, 516.
- [21] C.-Z. Chang, W. Zhao, D. Y. Kim, H. Zhang, B. A. Assaf, D. Heiman, S.-C. Zhang, C. Liu, M. H. W. Chan, J. S. Moodera, *Nat. Mater.* **2015**, 14, 473.
- [22] X. Kou, L. Pan, J. Wang, Y. Fan, E. S. Choi, W.-L. Lee, T. Nie, K. Murata, Q. Shao, S.-C. Zhang, K. L. Wang, *Nat. Commun.* **2015**, 6, 8474.
- [23] T. Nozaki, M. Oida, T. Ashida, N. Shimomura, T. Shibata, M. Sahashi, *Appl. Phys. Lett.* **2014**, 105, 212406.
- [24] F. Wang, D. Xiao, W. Yuan, J. Jiang, Y.-F. Zhao, L. Zhang, Y. Yao, W. Liu, Z. Zhang, C. Liu, J. Shi, W. Han, M. H. W. Chan, N. Samarth, C.-Z. Chang, *Nano Lett.* **2019**, 19, 2945.
- [25] W. Echtenkamp, Ch. Binek, *Phys. Rev. Lett.* **2013**, 111, 187204.
- [26] S. Cao, X. Zhang, N. Wu, A. T. N'Diaye, G. Chen, A. K. Schmid, X. Chen, W. Echtenkamp, A. Enders, C. Binek, P. A. Dowben, *New J. Phys.* **2014**, 16, 073021.
- [27] B. J. Kirby, P. A. Kienzle, B. B. Maranville, N. F. Berk, J. Krycka, F. Heinrich, C. F. Majkrzak, *Curr. Opin. Colloid Interface Sci.* **2012**, 17, 44.
- [28] B. Maranville, W. Ratcliff II, P. Kienzle, *J. Appl. Crystallogr.* **2018**, 51, 1500.